ISSN 0016-7932, Geomagnetism and Aeronomy, 2008, Vol. 48, No. 2, pp. 187–200. © Pleiades Publishing, Ltd., 2008.
Original Russian Text © E.L. Afraimovich, E.I. Astafyeva, I.V. Zhivetiev, A.V. Oinats, Yu.V. Yasyukevich, 2008, published in Geomagnetizm i Aeronomiya, 2008, Vol. 48, No. 2, pp. 195–208.

Global Electron Content during Solar Cycle 23

E. L. Afraimovich[a], E. I. Astafyeva[a], I. V. Zhivetiev[b], A. V. Oinats[a], and Yu. V. Yasyukevich[a]

[a] *Institute of Solar–Terrestrial Physics, Siberian Branch, Russian Academy of Sciences (ISZF SO RAN), P.O. Box 291, Irkutsk, 664033 Russia*

[b] *Institute of Cosmophysical Research and Radiowave Propagation, Far East Division, Russian Academy of Sciences, Mirnaya ul. 7, Paratunka, Elizovo raion, Kamchatka oblast, 684034 Russia*

Received March 23, 2007; in final form, July 26, 2007

Abstract—Global electron content (GEC) as a new ionospheric parameter was first proposed by Afraimovich et al. [2006]. GEC is equal to the total number of electrons in the near-Earth space. GEC better than local parameters reflects the global response to a change in solar activity. It has been indicated that, during solar cycle 23, the GEC dynamics followed similar variations in the solar UV irradiance and $F_{10.7}$ index, including the 11-year cycle and 27-day variations. The dynamics of the regional electron content (REC) has been considered for three belts: the equatorial belt and two midlatitude belts in the Northern and Southern hemispheres (±30° and 30°–65° geomagnetic latitudes, respectively). In contrast to GEC, the annual REC component is clearly defined for the northern and southern midlatitude belts; the REC amplitude is comparable with the amplitude of the seasonal variations in the Northern Hemisphere and exceeds this amplitude in the Southern Hemisphere by a factor of ~1.7. The dayside to nightside REC ratio, $R(t)$, at the equator is a factor of 1.5 as low as such a GEC ratio, which indicates that the degree of nighttime ionization is higher, especially during the solar activity maximum. The pronounced annual cycle with the maximal $R(t)$ value near 8.0 for the winter Southern Hemisphere and summer Northern Hemisphere is typical of midlatitudes.

PACS numbers: 94.20.wh, 96.60.Rd

DOI: 10.1134/S0016793208020084

1. INTRODUCTION

The Earth's ionosphere is an important part of the near-Earth space, the state of which depends on the solar irradiances at different wavelengths [Ivanov-Kholodny and Nikol'skii, 1969; Akasofu and Chapman, 1972; Krinberg and Tashchilin, 1984]. Beginning from the classical work [Beynon and Brown, 1959], many researchers have tried to restore the solar radiation characteristics based on the observations of the state of the ionosphere [Nusinov, 2004]. The necessity of solving this problem remains actual in spite of the development of the advanced extra-atmospheric (satellite) equipment for detecting solar radiation. Similar studies become of special importance in the present-day stage of development of the solar–terrestrial physics, when several extremely actual problems of the solar activity dynamics should be solved.

At present, different facilities for ground-based and satellite radiosounding are used to monitor the ionosphere [Bryunelli and Namgaladze, 1988]. Local characteristics of the ionosphere with substantial global distinctions are most often determined in this case. On the other hand, it is necessary to adequately use experimental data, obtained with the help of advanced facilities for monitoring solar radiation, in order to improve ionospheric models of different class [Bilitza, 2001]. These models are widely used to perform ionospheric studies and to maintain effective functioning of ground-based and satellite radio systems.

A new approach to the restoration of the solar radiation characteristics by determining GEC, equal to the total number of electrons in the near-Earth space limited by the GPS satellite orbit (about 20 200 km), was proposed in ISZF SO RAN [Afraimovich et al., 2006a]. The advantage of such an approach consists in that local specific features of ionospheric characteristics become smoothed, and regularities characterizing the GEC dynamics are revealed in a final analysis. At the same time, absolute values of GEC as a new ionospheric parameter are of independent interest since they have been obtained within the scope of a simple and physically substantiated model of refraction coefficient for ionospheric plasma [Hofmann-Wellenhof et al., 1992]. This model relates the values of the phase and group delay of GPS signals to the value of the total electron content in a column between a receiver and GPS satellite. From this viewpoint, experimental GEC values rank with electron density values at E or $F2$ region maximums, which are determined from measurements of the critical frequency at ionospheric stations.

2. GEC DETERMINATION METHOD

The method for determining GEC is first of all based on the usage of the technique for drawing global

ionospheric maps developed at several laboratories (JPLG, USA; CODG, Switzerland; and others). Global maps of the total electron content (global ionospheric maps, GIMs) are calculated based on the data of the international network of GPS receivers [Mannucci et al., 1998; Shaer et al., 1998] at different scientific centers, including: Geodetic Survey Division of Natural Resources Canada (EMRG) [http://www.nrcan.rncan.gc.ca/]; Center for Orbit Determination in Europe, University of Berne, Switzerland (CODG) [http://www.cx.unibe.ch/]; Jet Propulsion Laboratory of California Institute of Technology (JPLG) [http://www.jpl.nasa.gov/]; Grup Universitat Politecnica de Catalunya (UPCG) [http://www.upc.es/]; European Space Agency Group (ESAG); and others.

The algorithms for restoring the spatial–temporal distribution of the total electron content (TEC), developed at the above scientific centers, are described in detail in several publications [Mannucci et al., 1998; Schaer et al., 1998]. These algorithms are different; however, the general conception of restoration of the TEC absolute vertical value is based on the choice of optimal parameters of the selected model of electron density vertical distribution ($N(h)$ profile). The values of the anticipated ionospheric correction to a distance to GPS satellite for real angles of sight to GPS satellite are calculated for such a model. The calculated correction values are subsequently compared with the measured values, and this process is repeated for different parameters until minimal discrepancy values are obtained. The vertical TEC, which is essentially equal to the average TEC value for the corresponding GIM cell, is subsequently calculated for the $N(h)$ profile optimal for a discrepancy minimum.

The spatial range of GIMs, presented on the Internet site ftp://cddisa.gsfc.nasa.gov/pub/gps/products/ionex/ in the IONEX standard format, is 0°–360° in longitude and –90°to 90° in latitude; the size of GIM elementary cell is 5° in longitude and 2.5° in latitude. For each instant with a 2-h time resolution, from the IONEX files we obtained the vertical TEC values ($I_{i,j}$), where i and j subscripts show coordinates (latitude and longitude) of a GIM cell. Global electron content $G(t)$ is calculated by taking the sum of TEC values for each cell, multiplied into a GIM cell area ($S_{i,j}$), over all GIM cells [Afraimovich et al., 2006a, 2006b]

$$G = \sum S_{i,j} I_{i,j}. \quad (1)$$

The GIM cell area in the expression (1) is determined by using the formulas of spherical trigonometry at the Earth's surface level ($h = 0$). The error of such a GEC determination is presented in Section 3. To make an analysis of GEC more convenient, we proposed the GEC unit (GECU), equal to 10^{32} electrons [Afraimovich et al., 2006a], by analogy with the commonly accepted TEC unit (TECU). It is rather difficult to generally estimate the GEC calculation accuracy based on the known accuracy of TEC determination in each GIM cell in the initial IONEX file (the rms deviation of TEC determination in a GIM cell varies from 10 to 20% [Mannucci et al., 1998; Schaer et al., 1998]). This is related to a low spatial resolution of GIMs and to an irregular location of GPS receivers, as a result of which one should use spatial interpolation. The GEC calculation accuracy can be more or less reliably quantitatively estimated by comparing data from different laboratories which deliver maps to the Internet (see below).

We should note that the regional TEC maps with a higher spatial resolution have recently appeared: the *US TEC* North-American map [http://www.ngdc.noaa.gov/stp/IONO/USTEC/home.html], time resolution 15 min, spatial resolution 1° in latitude and longitude; the European map [http://ionosphere.rcru.rl.ac.uk/cgi-bin/SWWpagedis.pl?page=TEC/TEC_index&sel=2], time resolution 10 min, spatial resolution 1°; the *LPIM* South-American map [http://cplat.fcaglp.unlp.edu.ar/products/grids/], time resolution 1 h, spatial resolution 1°; the Japanese map [http:// wdc.nict.go.jp/IONO/contents/E011_ TEC-map.html], spatial resolution 0.5°, time resolution 5 and 15 min; and others. Thus, in near future, the resolution of TEC maps will be quite acceptable for more exact calculations of GEC since signals from other navigation systems (GLONASS, GALILEO) are used and the global and regional networks widen.

The GIM database for the period 1996–2006 presented in the Internet [ftp://cddisa.gsfc.nasa.gov/pub/gps/products/ionex/; http://www.cx.unibe.ch/] is the experimental basis for the present work. The calculations for the period June 1, 1998–September 1, 2006 (3014 days) were performed based on GIMs with the 2-h resolution. The daily average TEC maps were used for the period from January1, 1996, to June 1, 1998 (822 days). Thus, the total number of the calculated GEC values was $3014 \times 12 + 822 = 36\,990$.

The TEC maps from 11 different laboratories are easily accessible [ftp://cddisa.gsfc.nasa.gov/pub/gps/products/ionex/] but only CODG [http://www.cx.unibe.ch/], JPLG [http://www.jpl.nasa.gov/], UPCG [http://www.upc.es/], and ESAG data cover the maximal time interval (1998–2006).

The relative deviation values ($dG/G = [G_{JPLG} - G_k]/G_{JPLG}$, %) of the JPLG data calculated in laboratory k and the rms deviations of these deviations (%) for 1999–2005 for the data from different laboratories, smoothed by the 10-day window, are presented in table. It is evident that the GEC relative deviation value varies from 3 to 16% depending on the solar activity level. The GEC deviation values were maximal when the solar activity level was minimal. At the same time, the rms deviation (dG/G) varies from 2 to 6% and

is maximal during the solar activity maximum (2000–2002).

We should note that, only due to the effect of global summing using formula (1), one managed to determine the systematic difference between the data from different laboratories within several percent, whereas the accuracy of vertical TEC determination in a GIM cell is not more than 10–20% [Mannucci et al., 1998; Schaer et al., 1998].

A comparative analysis indicated that the results of GEC calculation insignificantly depend on a laboratory, the data of which were used to estimate GEC. The data of JPL laboratory were used in further calculations. The data of CODE laboratory with the corresponding correction were used when the JPL data were absent. The CODG GIM data available from the internet [http://www.cx.unibe.ch/] for 1200 UT were used for the period 1996–1998.

3. ANALYSIS LIMITATIONS

First, the term "global electron content" was used because the entire Earth's surface is mapped. In reality, TEC in the ionospheric regions around the geographic poles is very approximately estimated on these maps. The NOR maps, presented on the site [http://www.kn.nz.dlr.de/daily/tec-np] by the N. Jakowski group, is more representative for these regions. However, the contribution of high-latitude regions to GEC is substantially lower than that of middle and low latitudes; thus, the G value, calculated using formula (1) in a first approximation, is sufficiently close to the total number of electrons around the Earth.

Second, the present work studies the GEC dynamics which is caused by a change in solar activity within the major part of cycle 23 (1996–2006) and by the solar rotation (27-day variations). Therefore, we smooth the $G(t)$ series by the 10-day time window. In so doing, we average the daily variations and level very important effects of faster variations in GEC during geomagnetic disturbances; these processes require special studies, which is outside the scope of the present work. Moreover, the 1-day window was used to perform smoothing in order to calculate correlation functions.

Third, the calculation of the number of electrons for an individual GIM cell using formula (1) is factually performed within a tube of a constant diameter

$$G = R_E^2 \Delta\varphi[\cos\theta - \cos(\theta + \Delta\theta)]I, \qquad (2)$$

where $\Delta\theta$ and $\Delta\varphi$ are the cell angular dimensions, and θ is the cell latitude; h_{max} is the upper integration limit; R_E is the Earth's radius; $I = \int_{R_E}^{R_E + h_{max}} N(r)dr$ is the vertical TEC value in a given cell GIM; and $N(r)$ is the electron density (i.e., spherical divergence is ignored). Thus, the systematic error appears when the absolute value of the total number of electrons in the near-Earth space is recalculated using formula (1).

Relative difference between the GEC values, calculated using the data from different laboratories, and the rmsd differences

Ser. no.	Year	JPLG–CODG, %	JPLG–UPCG, %	JPLG–ESAG, %
1	1999	14.8 ± 2.3	12.1 ± 3.4	16.9 ± 1.7
2	2000	13.7 ± 2.9	3.2 ± 3.3	12.6 ± 3.6
3	2001	10.5 ± 5.2	4.2 ± 2.7	9.8 ± 2.8
4	2002	5.3 ± 5.8	4.6 ± 5.8	10.8 ± 4.5
5	2003	7.0 ± 2.5	9.4 ± 5.9	13.4 ± 2.7
6	2004	10.7 ± 7.3	10.9 ± 3.8	16.1 ± 3.6
7	2005	13.1 ± 1.9	12.6 ± 2.3	15.8 ± 3.0

The exact number of electrons in the spherical layer of height h_{max} can be expressed by the integral of electron density $N(r, \theta, \varphi)$

$$G_{theor} = \int_{R_E}^{R_E + h_{max}} \int_0^\pi \int_0^{2\pi} N(r, \theta, \varphi) r^2 \sin\theta dr d\theta d\varphi. \qquad (3)$$

If we assume that the electron density profile within one GIM cell can be considered independent of angular coordinates θ and φ to a high accuracy, the expression for the number of electrons in a truncated spherical cone resting on a given cell will have the form

$$G_{theor} = \Delta\varphi[\cos\theta - \cos(\theta + \Delta\theta)] \int_{R_E}^{R_E + h_{max}} N(r) r^2 dr. \qquad (4)$$

It is clear that the r^2 multiplier is under the integration sign in formula (4); therefore, one should evidently know the shape of the electron density profile up to a satellite orbit altitude in order to exactly determine the number of electrons.

With regard to formulas (2) and (4), the relative error of GEC simulation in formula (1) for one cell can be determined using the formula

$$\varepsilon = \frac{G_{theor} - G}{G} \times 100\%$$
$$= \frac{\int_{R_E}^{R_E + h_{max}} N(r)(r^2 - R_E^2) dr}{R_E^2 \int_{R_E}^{R_E + h_{max}} N(r) dr} \times 100\%. \qquad (5)$$

Solid lines in Fig. 1 show the relative error (ε, %), calculated using formula (5) depending on the upper integration limit (h_{max}), where the shape of the elec-

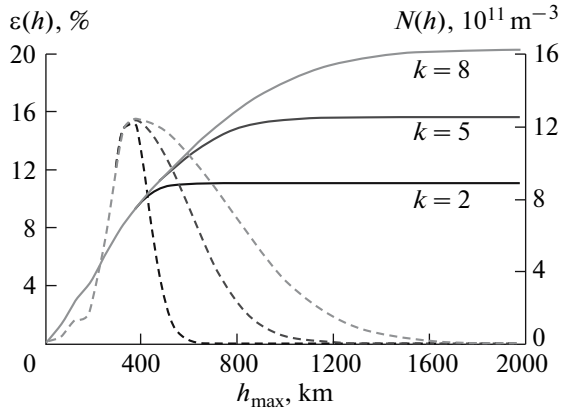

Fig. 1. Relative error (ε, %) of GEC calculation (solid lines) and the corresponding shapes of the electron density profile (dashed lines).

tron density profile (dashed lines in Fig. 1) from the NeQuick model [Leitinger et al., 2005] was used as a basis. Different curves correspond to different values of parameter k, which characterizes the rate of a decrease in the electron density above the $F2$ layer maximum according to the NeQuick model (black lines correspond to $k = 2$; dark gray lines, to $k = 5$; light gray, to $k = 8$). Figure 1 indicates that the relative error increases with increasing upper integration limit up to ~2000 km. Since the main number of electrons is located in the spherical layer at ionospheric altitudes from ~90 to ~1500 km, the growth of the error subsequently decelerates and tends to a certain limiting value of ~10–20%.

We should note that the above systematic error in determining the total number of electrons in the near-Earth space according to formula (1) mainly affects only the GEC absolute value rather than the form and character of GEC variations.

4. SOLAR ACTIVITY AND IONOSPHERE DURING CYCLE 23

4.1. Solar Activity Cycle

The data on the solar UV irradiance $U(t)$ in the range 0.1–50 nm, measured at SEM/SOHO space station [Judge et al., 1998; http://www.usc.edu/dept/space–science/semdatafolder/] and averaged over the entire solar disk, are used as an index of solar activity.

Since the data on the UV irradiance are not continuous, we also use the $F_{10.7}$, $F(t)$, index of solar activity, which is considered as good indicator of the HF solar radiation intensity [Ivanov-Kholodny and Nikol'skii, 1969]. The $F_{10.7}$ index is equal to the solar radiation flux at a wavelength of 10.7 cm in sfu (10^{-22} W m^{-2} Hz^{-1}). This index is often used in different ionospheric models (e.g. [Bilitza, 2001]) since $F_{10.7}$ can be measured on the Earth's surface, and long continuous series of measurements are already available [http://www.drao-ofr.hia-iha.nrc-cnrc.gc.ca/]. The R_{sn} index, characterizing the relative number of sunspots, is an important indicator [http://sidc.oma.be/ sunspot-data/].

To study the general pattern of the GEC variation dynamics, we used a wavelet analysis [Torrence and Compo, 1998]. The Butterworth bandpass filter [Krivitskii, 1977] was used to quantitatively estimate the GEC variation amplitude in different ranges of periods. Figure 2 presents the initial series of GEC smoothed by the 10-day time window (panel a), the $F_{10.7}$ index (panel b), and UV irradiance (panel c). The $G(t)$ dependence demonstrates that GEC substantially varied during cycle 23 (from 0.5 to 3.2 GECU).

Figure 3 shows the regression dependences of GEC on the UV irradiance (panels a, c) and $F_{10.7}$ index (panels b, d) constructed for the initial data (Fig. 2). Gray curves show the approximating functions; vertical bars in panels (c) and (d), the rms deviation (rmsd) values. We can see in Fig. 3a that the GEC and UV values are linearly dependent with an insignificant rmsd of about 20% (Fig. 3c). The scatter of the GEC and $F_{10.7}$ regression dependence is substantially larger (rmsd ~ 50%). Moreover, Figs. 3b and 3d indicate that the GEC saturation effect takes place at large $F_{10.7}$ values. This is in agreement with the results obtained by Liu et al. [2006], who analyzed long series of daily $F_{10.7}$ values and electron densities at an $F2$ layer maximum ($NmF2$) based on the data of 20 ionosondes. Liu et al. [2006] revealed the effect of $NmF2$ saturation at large $F_{10.7}$ values. This, specifically, means that the error appears in the calculations of the ionospheric parameters at high levels of solar activity if $F_{10.7}$ is used in ionospheric models.

A comparison between the variations in GEC and in the $F_{10.7}$ index of solar activity (Figs. 2a, 2b) indicated that the $G(t)$ dependence is in good agreement with $F(t)$. This is especially evident when the $G(t)$ and $F(t)$ dependences smoothed by the 1-year time window are compared (Fig. 4; black and gray curves, respectively). Figure 4 also presents for comparison the time variations, $R_{sn}(t)$, in the relative number of sunspots R_{sn} (dashed curve) smoothed by the 1-year window, which demonstrates good agreement with both $G(t)$ and $F(t)$.

The regression dependence of the GEC values on the UV irradiance for the period 1998–2006, smoothed by the 1-year time window, is approximated by the linear function

$$G = 4.16U - 0.3. \quad (8)$$

The regression dependence of the GEC values on $F_{10.7}$, smoothed by the 1-year time window, is also approximated by the linear function

$$G = 0.01F - 0.3. \quad (9)$$

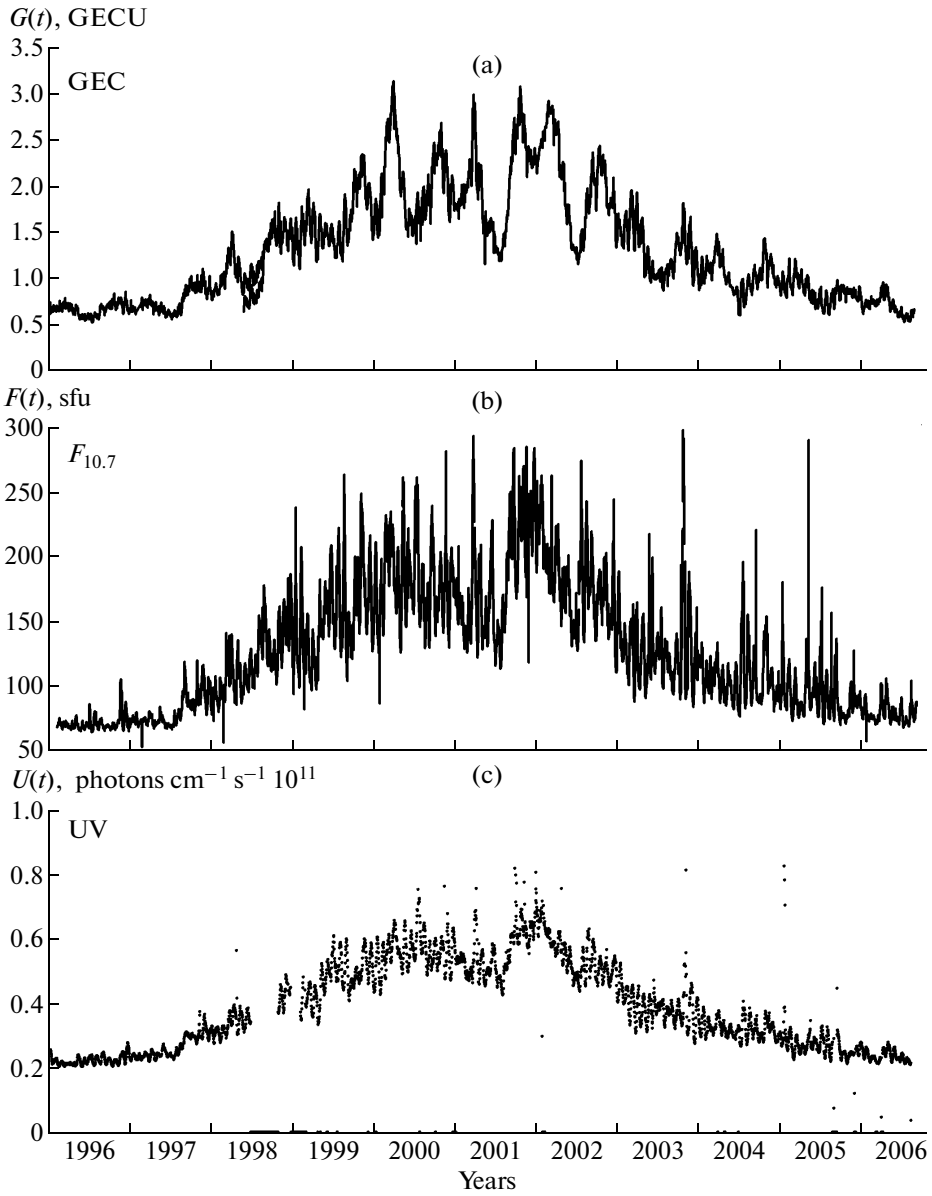

Fig. 2. Variations in (a) GEC, (b) $F_{10.7}$ solar activity index, and (c) UV irradiance during cycle 23 (1996–2006).

The presented relationships are in rather good agreement with similar formulas for critical frequencies of the ionospheric *F*2 layer, accepted in modern empirical models of the ionosphere [Bryunelli and Namgaladze, 1988].

4.2. Semiannual Variations

An analysis of the $G(t)$ time series indicated that strong seasonal (semiannual) variations are typical of GEC. This is clearly defined in the dynamic spectrum of GEC variations obtained with the help of a wavelet transform (Fig. 5a). The dynamic spectra of the UV and $F_{10.7}$ variations are presented in Fig. 5 for comparison (panels b and c, respectively). The relative amplitude of the GEC seasonal variations changes from 10 to 30% when solar activity increases and decreases during the period of maximum, respectively. This is illustrated by the variations in the relative amplitude of $dG(t)/G(t)$ (black curve) and $dF(t)/F(t)$ (gray curve) filtered in the range of periods from 100 to 300 days.

Figure 6 indicates that the GEC seasonal variations are maximal at the end of March–beginning of April and at the end of October–beginning of November, i.e., during the periods of equinox. This is in rather good agreement with the fact that the density of the neutral atmosphere at ionospheric altitudes is maximal in April and October [Krinberg and Tashchilin, 1984; Oyama et al., 2005]. As one would expect, the

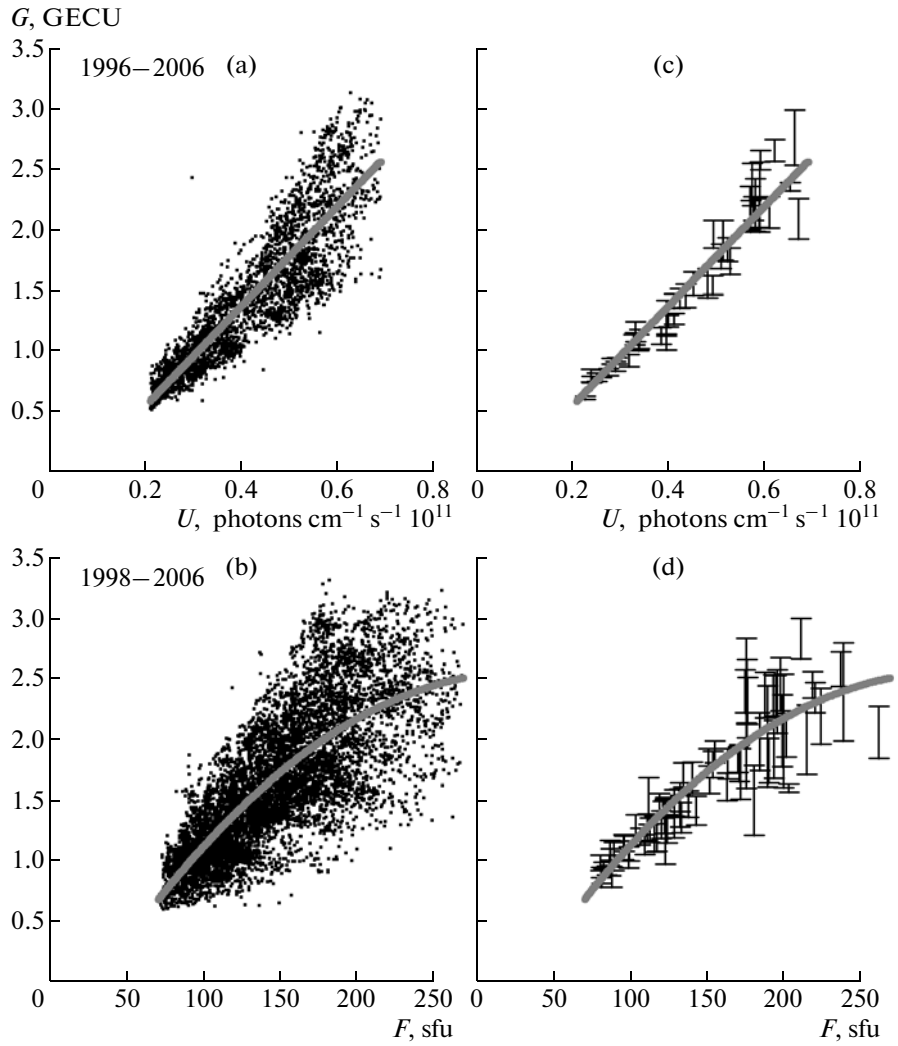

Fig. 3. Regression dependences of GEC values on (a) and (c) UV and (b) and (d) $F_{10.7}$; gray curves show the approximating dependences, and vertical bars in panels (c) and (d) indicate the rmsd values.

semiannual variations in GEC and $F_{10.7}$ do not correlate.

4.3. Day–Night Variations

To understand the physical mechanisms, it is very important to determine GEC, independently for the day (G_d) and night (G_n) sides of the Earth, and the ratio of these quantities ($R_G = G_d/G_n$). To estimate G_d and G_n, we make the summation, using formula (1), only for GIM cells that are located on opposite sides of the solar terminator line determined for the specified altitude in the atmosphere. The calculations were performed for an altitude of $H = 200$ km, which is close to the range of altitudes where the ionization of the atmosphere by the solar UV radiation is most intense [Bryunelly and Namgaladze, 1988].

Figure 7a presents the GEC values on the day $G_d(t)$ and night $G_n(t)$ sides of the Earth (gray and black curves, respectively) smoothed by the 10-day window. Figure 7b illustrates the time variation in the $R_G(t)$ ratio during cycle 23, smoothed by the 81-day time window; smoothing was performed in order to suppress the effects caused by the solar rotation. The R_G value varied from 3 to 3.5 with increasing solar activity and was equal to 2.8–3.4 at an activity maximum. Figure 7b indicates that the $R_G(t)$ and $G(t)$ values show deep seasonal variations; however, the $G(t)$ maximal values are observed during the solstice periods (in winter and summer) in contrast to $R_G(t)$. Such a seasonal variation is qualitatively related to the Earth's axis inclination with respect to the ecliptic plane, and quantitative relationships require modeling.

A comparison with the data of the IRI-2001 empirical model [Afraimovich et al., 2006b], performed by

us, indicated that the IRI-2001 model gives pronouncedly underestimated values of the $R_G(t)$ ratio as compared to the experimental data. This means that the degree of nightside ionization in the IRI-2001 model is strongly overestimated. However, the obtained data can be soundly interpreted only using physical ionospheric models such as, e.g., the [Krinberg and Tashchilin, 1984] model. This procedure is outside the scope of our paper.

4.4. 27-Day Variations

The 27-day variation caused by the solar rotation is one of the important factors of the solar radiation effect on the state of the ionosphere. Many works are devoted to studying this factor [Akasofu and Chapman, 1972; Ivanov-Kholodny and Nikol'skii, 1969; Vitinsky et al., 1986; Jakowski et al., 1991, 2002]. However, the 27-day modulation of the ionospheric parameters measured at one point is masked by numerous other factors, which hinders obtaining reliable quantitative characteristics of the 27-day variation in solar ultraviolet. GEC more distinctly reflects this specific feature of the ionospheric dynamics related to the solar rotation.

Figure 8a demonstrates the dynamic wavelet (the spectrum of $G(t)$ variations), where the 27-day component of GEC variations during the phases of solar activity growth and decline is clearly defined. The dynamic spectra of the $F_{10.7}$ and UV variations are presented for comparison in Figs. 8b and 8c, respectively.

The 27-day variations in $dG(t)$ (gray curves), $dF(t)$ (black curves), and $dU(t)$ (dashed curves) are presented in Figs. 9a–9c for the period from June 1, 2003, to May 18, 2004. This period includes the time interval when strong heliospheric disturbances of October–November 2003 were registered [Veselovsky et al., 2004].

A correlation analysis of the data for 1999–2006 revealed a high degree of similarity between the 27-day variations in the $G(t)$, $F(t)$, and $U(t)$ series obtained by filtering the initial series in the range of periods 20–40 days. The correlation coefficient between GEC and UV reaches 0.94, and the correlation coefficients between the GEC and $F_{10.7}$ as well as between $F_{10.7}$ and UV are slightly lower (0.83 and 0.79, respectively). The cross-correlation functions $\rho(\tau)$ of the corresponding series for $N = 102$ solar rotations are shown in Fig. 10a, which indicates that the 27-day variations in GEC, $dG(t)$, on average lag behind the corresponding variations in $F_{10.7}$ and UV by two days, and the $dF(t)$ and $dU(t)$ variations are in phase.

Let us consider in more detail the histograms of the relative delay of the 27-day variations, $N(\tau)$, between the $dG(t)$, $dF(t)$, and $dU(t)$ series (Figs. 10b–10d). The most probable and average delay values ($\tau = 2$ days), determined from the histograms shown in Figs. 10c and 10d, are close to the delay of the maximum of the

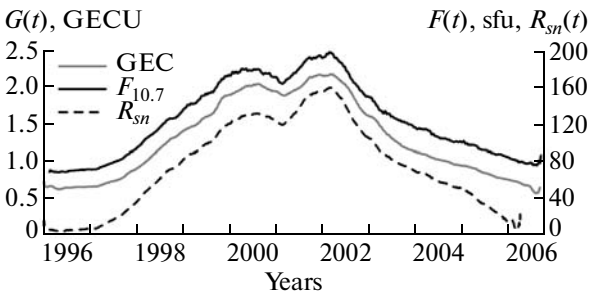

Fig. 4. The variations in GEC (gray curve), $F_{10.7}$ (black curve), and the relative number of sunspots R_{sn} (dashed line) smoothed by the 1-year time window.

$\rho(\tau)$ cross-correlation functions presented in Fig. 10a. The average value of the delay (τ) between the GEC and UV variations is 2.2 days with an rmsd of 1.4 days, and the value of such a delay between GEC and $F_{10.7}$ is 1.76 days with an rmsd of 2.5 days. This can be caused by the fact that the 27-day variations in $F_{10.7}$ systematically lead such variations in UV on average by 0.46 days with an rmsd of 2.2 days. It is difficult to detect this lead on the corresponding correlation function in Fig. 10a because of a considerable scatter of the delay between the $F_{10.7}$ and UV series (Fig. 10b). As a consequence, the scatter of the delay between $dG(t)$ and $dF(t)$ considerably exceeds the scatter between $dG(t)$ and $dU(t)$, which quite agrees with the conclusion that the correlation between the GEC and UV series is closer than the correlation between GEC and $F_{10.7}$ (Section 4.1).

Our results agree with the data obtained by Nusinov and Katyushina [1994], who indicated that the variations in the UV irradiance (130–210 nm) lag behind the $F_{10.7}$ index as a rule by a day. These researchers assumed that this delay can be caused by two factors: (1) by a difference between the rate of fading of local solar sources in the UV range and at a wavelength of 10.7 cm; (2) by different conditions of visibility of formations on the solar limb, when the region of UV generation is already outside the limb and the corresponding region of radio emission has not yet been shaded by the Sun. A certain difference between our results and the data obtained in [Nusinov and Katyushina, 1994] can be related to the fact that different time intervals (1982–1988 and 1996–2006) and UV radiation bands (130–210 and 0.1–50 nm) were selected for study.

Thus, the 27-day GEC variations on average lag behind the corresponding variations in $F_{10.7}$ and UV by 2 days (see Figs. 9, 10). It is known that the response of the ionosphere to the variations in the UV irradiance depends on the time constants of ionization and recombination (about an hour) [Ivanov-Kholodny and Nikol'skii, 1969; Bryunelli and Namgaladze, 1988]. The delay of the 27-day GEC variations relative to the corresponding variations in the $F_{10.7}$ and UV

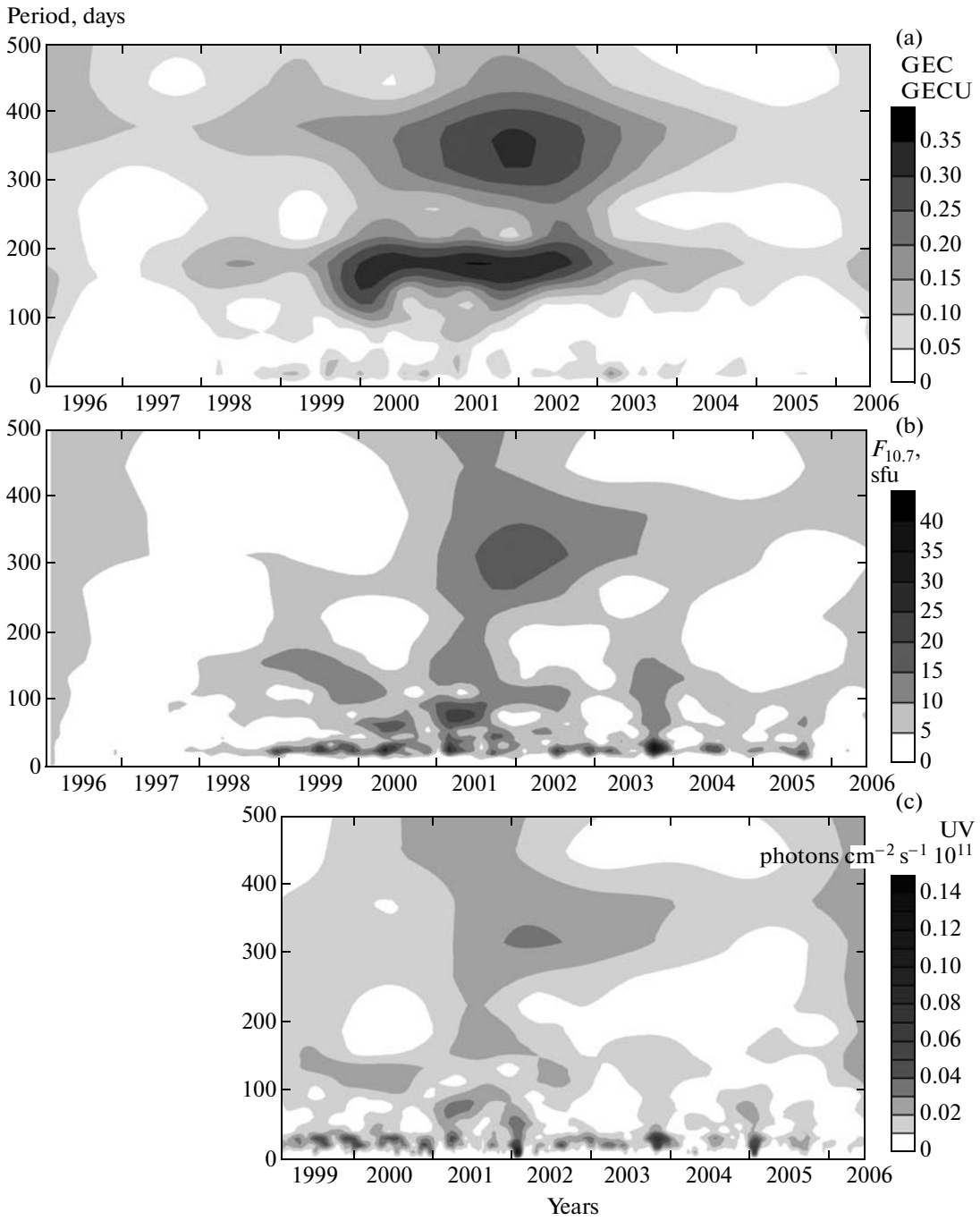

Fig. 5. The dynamic spectrum of variations in (a) GEC, (b) $F_{10.7}$, and (c) UV in the range of periods up to 500 days.

irradiances can be caused by substantially larger time constants, typical of the thermosphere, since GEC variations are caused by not only variations in the solar ionizing radiation but also by the processes in the thermosphere. The temperature and total density of the atmosphere increase, and the neutral wind velocity and direction change with increasing solar irradiance, which ionizes the ionosphere and heats the thermosphere [Bryunelli and Namgaladze, 1988]. It is also necessary to take into account that the time scales of variations in the electron content in the Earth's plasmasphere vary from 2 to 5 days [Krinberg and Tashchilin, 1984]. A detailed analysis of the factors responsible for the detected delay of the 27-day variations is a very complex problem and is outside the scope of the present work.

It is very important to estimate the dependence of the envelop of the 27-day variation relative, $G27(t)$,

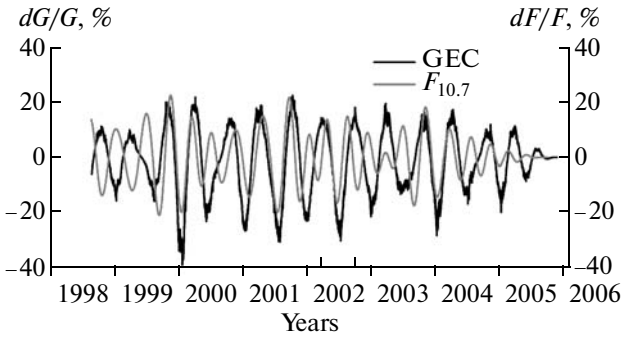

Fig. 6. Variations in the $dG(t)/G(t)$ and $dF(t)/F(t)$ relative amplitudes filtered in the range of periods 100–300 days.

amplitude during the solar cycle. At the first stage, we calculated the $dG(t)/G(t)$ dependence by normalizing the initial GEC series, $dG(t)$, filtered in the range of periods 20–40 days, to the background $G(t)$ values. Then, we squared the $dG(t)/G(t)$ series and smoothed them by the 81-day time window. The time dependence of the envelop of the 27-day variations in the $F_{10.7}$ index, $F27(t)$, was calculated in the same way.

Figure 11b presents the $G27(t)$ (gray curves) and $F27(t)$ (black curves) time dependences during cycle 23 (1996–2006) smoothed by the 365-day time window. The smoothed $F_{10.7}$ dependence (black curve) and the dependence of the daily average values of the relative sunspot number R_{sn} (dashed curve) are shown in Fig. 11a for the period from 1996 to 2006. The maximal deviation of the amplitude of the 27-day GEC variations, $G27(t)$, changes from 8% during the solar activity growth and decline to 2% during the periods of activity maximum and minimum. At the same time, the amplitude of the 27-day variations in the $F_{10.7}$ index during the periods of solar activity growth and decline reaches 12–14%.

Such a regularity is caused by the specific features of active formations on the Sun's surface, the number of which increases with increasing solar activity [Mordvinov and Plyusnina, 2001; Mordvinov and Willson, 2003]. The amplitude of the 27-day modulation of the UV irradiance increases in this case. During the period of solar activity growth and, especially, decline frozen-in intense active formations, which can exist during several solar rotations, are generated on the Sun's surface [Vitinsky et al., 1986; Mordvinov and Plyusnina, 2001; Mordvinov and Willson, 2003]. For a single frozen-in active formation, the solar UV irradiance crosses only once the Sun–Earth line during one solar rotation. Thus, the $U(t)$ dependence has only one maximum, which causes strong GEC fluctuations with the period equal to the period of solar rotation. Many active formations are generated and constantly move over the Sun's surface at a high level of solar activity. In spite of the fact that the average modulation amplitude of the $U(t)$ function increases in this

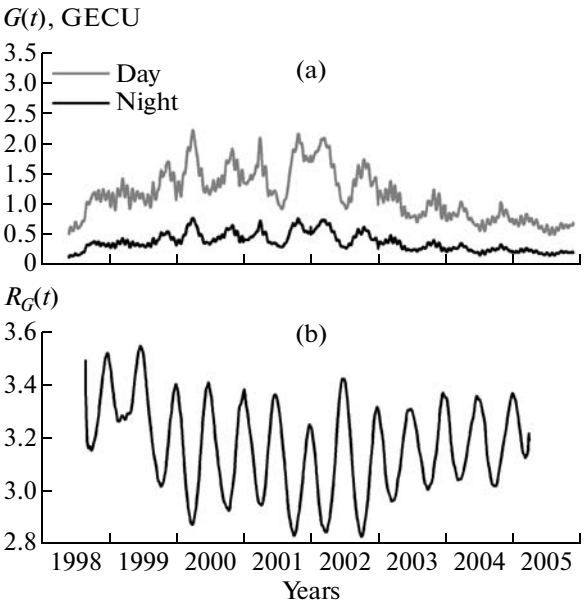

Fig. 7. (a) The GEC values on the night (black curve) and day (gray curve) sides of the Earth smoothed by the 10-day window; (b) the dependence of the $R_G(t)$ ratio of GEC on the dayside to such a ratio on the nightside of the Earth.

case, the relative amplitude of 27-day variations, on the contrary, decreases. The minimal level of the 27-day modulation is also observed during the period of low solar activity, when the number of active formations is minimal (tends to zero).

Figure 12 shows the dependences of the $EdG(t)$, $EdF(t)$, and $EdU(t)$ envelops, which are the tangents to the maximums of the $dG(t)$, $dF(t)$, and $dU(t)$ 27-day variations shown in Fig. 9. As was mentioned above, strong heliospheric disturbances of October–November 2003 were registered during this period. The horizontal dashed line shows the level of half-maximums of the 27-day variation envelops; arrows, the time intervals (DT) during which the envelop value exceeded the level 0.5. The DT values can be used to estimate the lifetime of frozen-in active formations on the Sun, which emit in different wavelength ranges. Figure 12 indicates that the intensities of the 27-day variations in $F_{10.7}$, UV, and GEC started increasing almost synchronously, with a difference of several days. The intensities of the $dG(t)$ and $dU(t)$ variations decreased also synchronously but with a delay of about 30 days relative to the $dF(t)$ variations. The established delay can be related to a difference in the origin and spatial–temporal characteristics of the solar radiation in the UV and radio ranges [Nusinov and Katyushina, 1994].

4.5. Electron Content in Geomagnetic Coordinates

In this section the electron content dynamics is considered on the regional scale, rather than on the

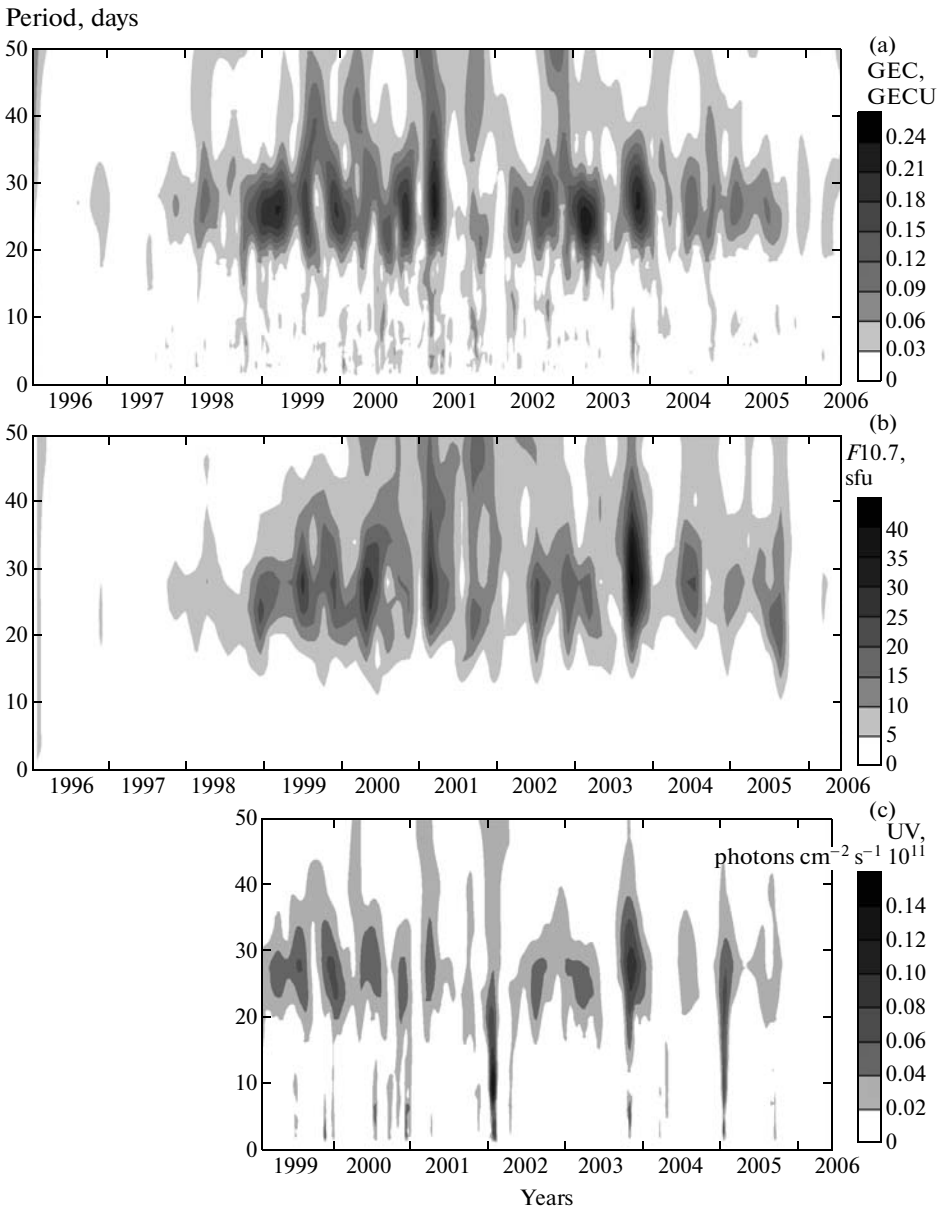

Fig. 8. The dynamic spectrum of the 27-day variations in (a) GEC, (b) $F_{10.7}$, and (c) UV in the range of periods up to 50 days.

global one, preferably in geomagnetic coordinates. At the first stage, we used the GIM data in geographic coordinates to determine REC. Then, the global TEC maps were transformed into geomagnetic coordinates. Based on the known geophysical concepts, we selected three main regions for analysis: the equatorial belt and midlatitude regions of the Northern and Southern hemispheres (±30° and 30°–65° geomagnetic latitudes, respectively). The auroral zones of the Northern and Southern hemispheres were not considered because TEC is estimated very approximately in the ionospheric regions around the geographic poles on GIMs. Moreover, it is impossible to adequately analyze the geophysical processes in these zones without data of the entire complex of experimental facilities including radar and optical ground-based and satellite monitoring systems.

We will analyze the specific dynamics in the midlatitude and equatorial region in comparison with the corresponding GEC characteristics. In Fig. 13a the GEC variations during cycle 23 smoothed by the 1-year window (dashed curve; see also Fig. 4) are presented together with the REC variations in the equatorial belt (panel a, gray curve) and in the midlatitude belts of the Northern and Southern hemispheres (panel b; gray and black curves, respectively). We should note that the dynamics of REC and GEC in these regions is on the whole rather similar, and the contribution of the equatorial belt to the global con-

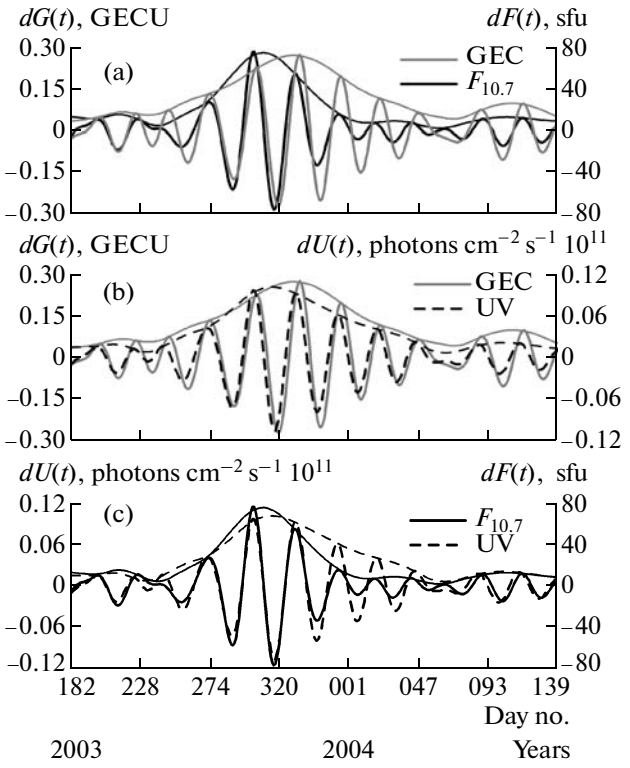

Fig. 9. The variations in (a) GEC and $F_{10.7}$, (b) GEC and UV, and (c) UV and $F_{10.7}$, smoothed in the range of periods 20–40 days from June 1, 2003, to May 18, 2004.

tent is determining (not less than 55%). However, a certain asymmetry in REC of the Northern and Southern hemispheres (Fig. 13b), reaching 2%, is typical of the period of solar activity maximum.

The seasonal variations in REC of the equatorial belt, filtered from the initial series in the range of periods 100–200 days (Fig. 13c), are almost the same as the GEC variations (Fig. 6). However, the annual component, filtered in the range 200–500 days (Fig. 13d), is also clearly defined for the Northern and Southern midlatitude belts. The amplitude of the annual REC variation is comparable with that of the seasonal variations in the Northern Hemisphere and is larger than the amplitude of the seasonal variations in the Southern Hemisphere by a factor of ~1.7.

The specific features of the $R(t)$ ratio of the electron content on the Earth's day and night sides for different regions substantially differ from the global regularities. For the equatorial belt, the $R(t)$ dependence is similar to $R_G(t)$ for the entire globe with an evident seasonal dependence and maximal values during the equinoxes (Fig. 14a; see also Fig. 7b). However, in contrast to $R(t)$ for REC, the $R(t)$ ratio for GEC at the equator is not more than 3.0 during the entire cycle 23, which indicates that the degree of nightside ionization is higher, especially during the solar activity maximum ($R(t) \sim 2.6$).

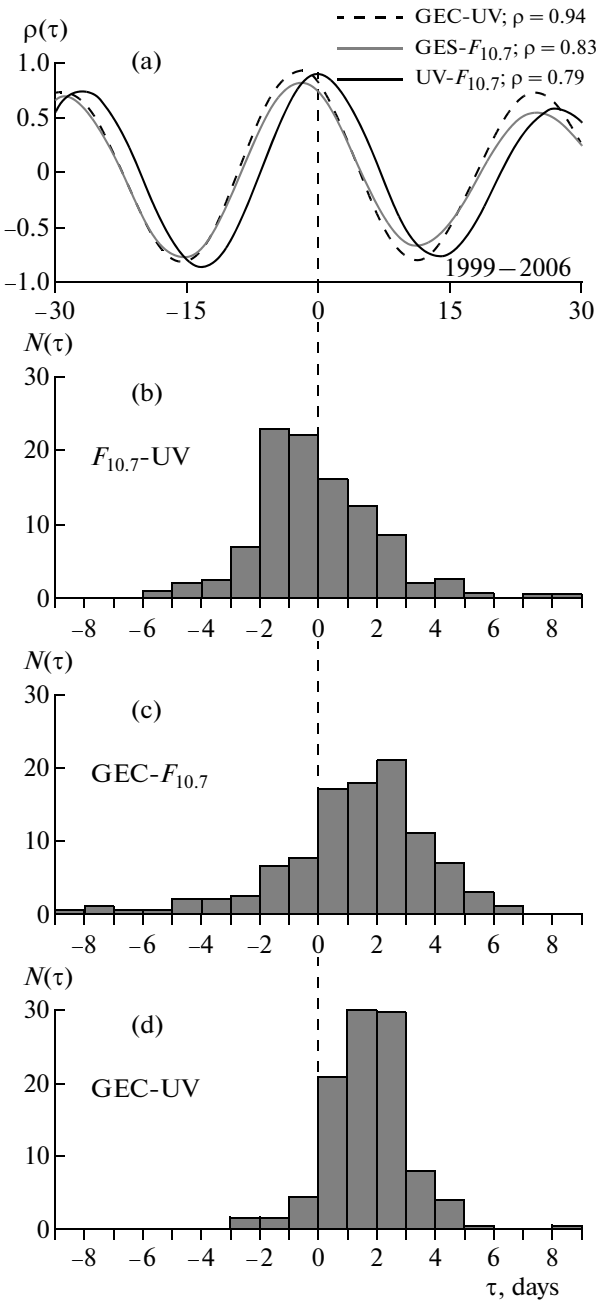

Fig. 10. (a) Cross-correlation functions of the GEC, UV, and $F_{10.7}$ series filtered in the range of periods 20–40 days. (b–d) The histograms of the relative delay of the 27-day variations.

The $R(t)$ differences are even more significant for midlatitudes in the Northern and Southern hemispheres, with the clearly defined annual cycle and the maximal value about 8.0 for the winter Southern Hemisphere and summer Northern Hemisphere and the minimal values about 3.0 (Fig. 14b). The absence of a pronounced dependence of $R(t)$ on the solar cycle for midlatitudes was unexpected. This fact can be

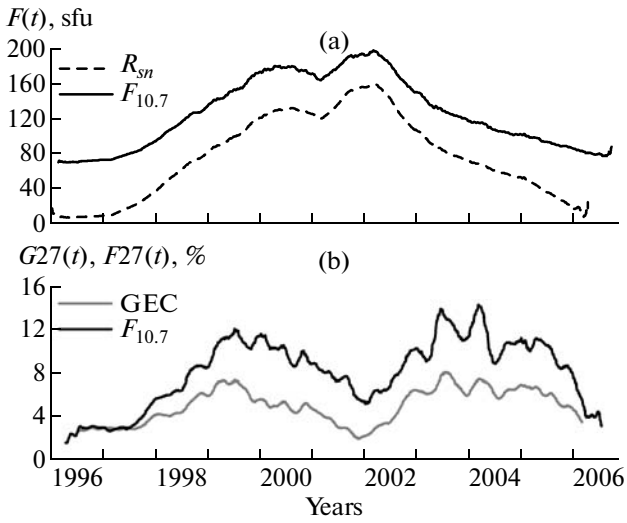

Fig. 11. (a) The dependences of the $F_{10.7}$ index (black curve) and the daily value of the relative sunspot number R_{sn} (dashed curve) smoothed by the 1-year time window; (b) the dependences of the envelop of the 27-day variations in GEC (gray curve) and $F_{10.7}$ (black curve).

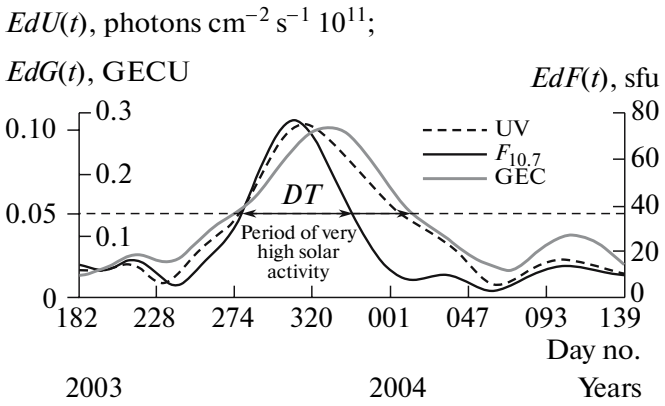

Fig. 12. Envelope (tangent to the maximums) of the 27-day variations in GEC, $F_{10.7}$, and UV from June 1, 2003, to May 18, 2004.

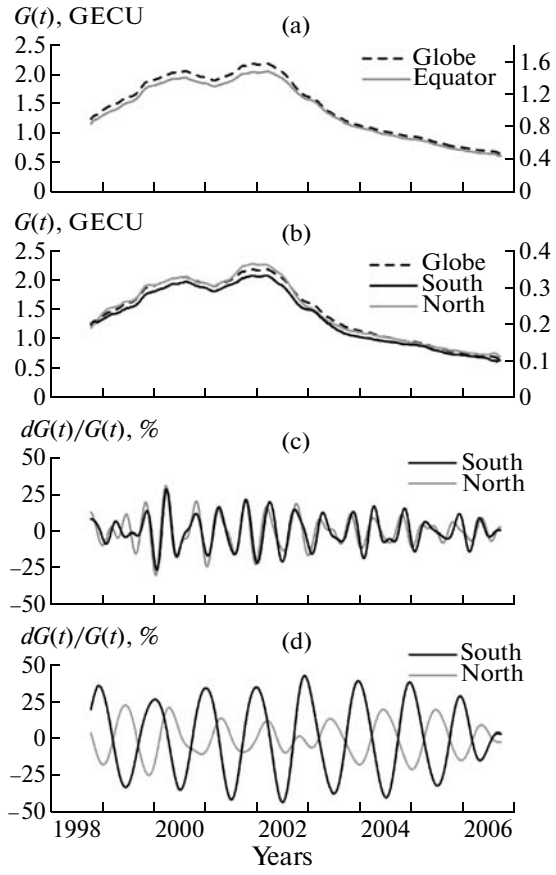

Fig. 13. A comparison of the GEC and REC dynamics during cycle 23: (a) and (b) the $G(t)$ dependences smoothed by the 1-year window; (c) and (d) the $dG(t)/G(t)$ semiannual and annual variations, respectively.

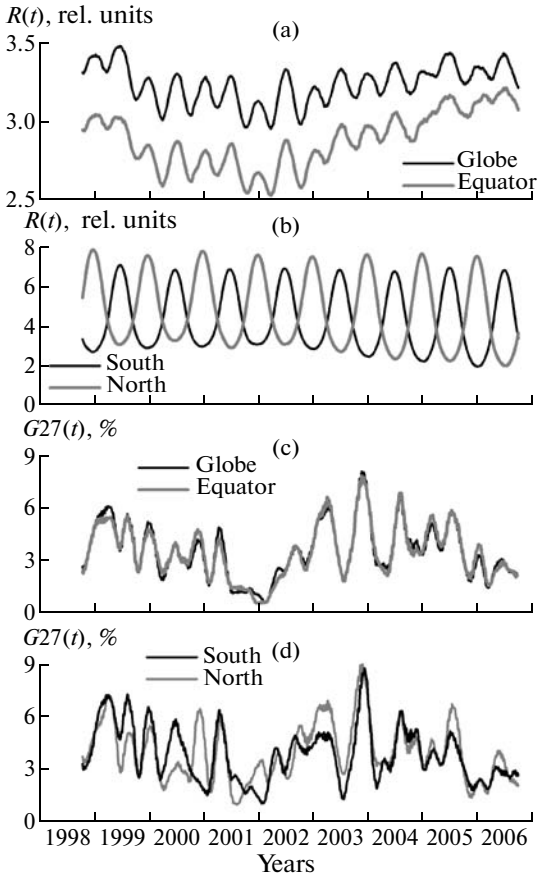

Fig. 14. (a) and (b) The $R(t)$ ratio for different regions during cycle 23; (c) and (d) the relative amplitude of the 27-day variations $G27(t)$ during cycle 23.

explained by a detailed numerical simulation, which is outside the scope of this paper.

The amplitude of the 27-day REC variations in the equatorial belt, $G27(t)$, almost follows the corresponding curve for GEC (Fig. 14c; see also Fig. 11b). Insignificant differences are observed only for midlatitudes, where the $G27(t)$ fluctuations are not phased (Fig. 14d).

The obtained results can be used to examine different ionospheric models. The differences in the main REC characteristics for different regions with substantially different geophysical conditions are qualitatively explained by the natural annual cycle of illumination at midlatitudes and by the specific features of the equatorial belt ionization. A quantitative analysis requires corresponding modeling.

5. CONCLUSIONS

We developed the method and programs for calculating a new ionospheric parameter—global electron content—using the GPS data. We established that GEC varied from 0.5 to 3.2 GECU during cycle 23 according to the dynamics of the solar UV irradiance and the $F_{10.7}$ index. Strong seasonal variations (to 30%), with the maximum during the periods of equinox, and the seasonal variations in the GEC ratio on the day and night sides of the Earth, with the maximums during the summer and winter solstices, are typical of GEC. The 27-day variations in GEC are similar to the corresponding variations in $F_{10.7}$ and UV (the correlation coefficient is larger than 0.9) but lag behind the later variations by 2 days on average. The relative amplitude of the 27-day variations decreases from 8% during the periods of solar activity growth and decline to 2% during the activity maximum and minimum, which qualitatively corresponds to the dynamics of active formations on the Sun during the 11-year cycle of solar activity.

The dynamics of the regional electron content during cycle 23 was considered for three belts: the equatorial belt and two midlatitude belts in the Northern and Southern hemispheres (±30° and 30°–65° geomagnetic latitudes, respectively). The annual component is clearly defined for the Northern and Southern hemispheres, and the amplitude of this component is comparable with that of the seasonal variations in the Northern Hemisphere and is larger than the amplitude of the seasonal variations in the Southern Hemisphere by a factor of ~1.7. The $R(t)$ ratio for equatorial REC on the Earth's dayside to such a ratio on the nightside is a factor of 1.5 as low as this ratio for GEC, which indicates that the degree of nightside ionization is higher, especially during the period of solar activity maximum. A clearly defined annual cycle, with the maximal $R(t)$ value about 8.0 for the winter Southern Hemisphere and summer Northern Hemisphere, is typical of midlatitudes. Such variations can be related to the natural annual cycle of illumination of the hemispheres.

The results obtained by us can be used to develop ionospheric models and to solve different problems of the solar–terrestrial coupling based on the observations of the ionosphere.

ACKNOWLEDGMENTS

We are grateful to G.A. Zherebtsov, V.I. Kurkin, A.V. Medvedev, V.G. Eselevich, A.V. Mordvinov, and L.A. Plyusnina for the interest to the work and useful discussion and to S.V. Voyeikov and I.N. Fedulina for the help in data processing.

This work was supported by the Russian Foundation for Basic Research (project no. 07-05-00127), RFFI-GFEN (project no. 06-05-39026), and SO RAN–DVO RAN–NANU (integration grant 3.24).

REFERENCES

1. E. L. Afraimovich, E. I. Astafyeva, and I. V. Zhivetiev, "Solar Activity and Global Electron Content," Dokl. Akad. Nauk **409** (3), 399–402 (2006a) [Dokl. Akad. Nauk **409A** (6), 921–924 (2006a)].
2. E. L. Afraimovich, E. I. Astafyeva, A. V. Oinats, et al., "Global Electron Content as a New Index of Solar Activity. Comparison with IRI Modeling Results," IRI News **13** (1A5) (2006b).
3. S.-I. Akasofu and S. Chapman, *Solar–Terrestrial Physics* (Pergamon, Oxford, 1972; Mir, Moscow, 1975).
4. W. J. G. Beynon and G. M. Brown, "Region *E* and Solar Activity," J. Atmos. Phys. **15**, 168–174 (1959).
5. D. Bilitza, "International Reference Ionosphere," Radio Sci. **36** (2), 261–275 (2001).
6. B. E. Bryunelli and A. A. Namgaladze, *Physics of the Ionosphere* (Nauka, Moscow, 1988) [in Russian].
7. *Handbook of Radio Electronics Theory*, Ed. by B. Kh. Krivitskii (Energiya, Moscow, 1977), Vol. 2 [in Russian].
8. B. Hofmann-Wellenhof, H. Lichtenegger, and J. Collins, *Global Positioning System: Theory and Practice* (Springer, New York, 1992).
9. G. S. Ivanov-Kholodny and G. M. Nikol'skii, *The Sun and the Ionosphere* (Nauka, Moscow, 1969) [in Russian].
10. N. Jakowski, S. Heise, A. Wehrenpfennig, et al., "GPS/GLONASS-Based TEC Measurements as a Contributor for Space Weather," J. Atmos. Sol.–Terr. Phys. **64** (5-6), 729–735 (2002).
11. N. Jakowski, B. Fichtelmann, and A. Jungstand, "Solar Activity Control of Ionosphere and Thermosphere Processes," J. Atmos. Terr. Phys. **53**, 1125–1130 (1991).
12. D. L. Judge, D. R. McMullin, H. S. Ogawa, et al., "First Solar EUV Irradiances Obtained from SOHO by the Celias/Sem," Sol. Phys. **177**, 161–173 (1998).
13. I. A. Krinberg and A. V. Tashchilin, *The Ionosphere and Plasmasphere* (Nauka, Moscow, 1984) [in Russian].

14. R. Leitinger, M. Zhang, and S. M. Radicella, "An Improved Bottom Side for the Ionosphere Electron Density Model NeQuick," Ann. Geophys. **48** (3), 525–534 (2005).
15. L. Liu, W. Wan, B. Ning, et al., "Solar Activity Variations of the Ionosphere Peak Electron Density," J. Geophys. Res., **111**, A08304 (2006).
16. A. J. Mannucci, B. D. Wilson, D. N. Yuan, et al., "A Global Mapping Technique for GPS-Derived Ionosphere TEC Measurements," Radio Sci. **33** (3), 565–582 (1998).
17. A. V. Mordvinov and L. A. Plyusnina, "Coherent Structures in the Dynamics of the Large-Scale Solar Magnetic Field," Astron. Zh. **78** (8), 753–760 (2001) [Astron. Rep. **45** (8), 652–658 (2001)].
18. A. V. Mordvinov and R. C. Willson, "Effect of Large-Scale Magnetic Fields on Total Solar Irradiance," Sol. Phys. **215**, 5–16 (2003).
19. A. A. Nusinov and V. V. Katyushina, "Lyman-Alpha Line Intensity as a Solar Activity Index in the Far Ultraviolet Range," Sol. Phys. **152**, 201–206 (1994).
20. A. A. Nusinov, "The Ionosphere as a Natural Detector for Studying Long-Period Variations in the Fluxes of Solar Geoeffective Radiation," Geomagn. Aeron. **44** (6), 779–786 (2004) [Geomagn. Aeron. **44**, 718–725 (2004)].
21. K.-I. Oyama, K. Noguchi, M. Izawa, et al., "Local Time, Annual, Latitude, and Seasonal Variations of Total Electron Content over Japan," ISAS Res. Note **796** (2005).
22. S. Schaer, G. Beutler, and M. Rothacher, "Mapping and Predicting the Ionosphere," in *Proceedings of the IGS AC Workshop, Darmstadt, 1998*, pp. 307–320.
23. C. Torrence and G. P. Compo, "A Practical Guide to Wavelet Analysis," Bull. Am. Meteorol. Soc. **79**, 61–78 (1998).
24. I. S. Veselovsky, et al., "Solar and Heliospheric Phenomena in October–November 2003: Causes and Consequences," Kosm. Issled. **42** (5), 453–508 (2004).
25. Yu. I. Vitinsky, M. Kopetsky, and G. V. Kuklin, *Statistics of Sunspot Formation Activity* (Nauka, Moscow, 1986) [in Russian].